Chemistry and Physics of Lipids 184 (2014) 119–128

Contents lists available at ScienceDirect

Chemistry and Physics of Lipids

journal homepage: www.elsevier.com/locate/chemphyslip

NMR-based molecular ruler for determining the depth of intercalants within the lipid bilayer. Part IV: Studies on ketophospholipids

Michal Afri, Carmit Alexenberg, Pinchas Aped, Efrat Bodner, Sarit Cohen, Michal Ejgenberg, Shlomi Eliyahu, Pessia Gilinsky-Sharon, Yifat Harel, Miriam E. Naqqash, Hani Porat, Ayala Ranz, Aryeh A. Frimer *

The Department of Chemistry, Bar-Ilan University, Ramat Gan 5290002, Israel

ARTICLE INFO

Article history:
Received 9 March 2014
Received in revised form 11 June 2014
Accepted 8 July 2014
Available online 23 July 2014

Keywords:
Liposome
^{13}C NMR
E_T
DMPC
Ketophospholipids
Molecular ruler

ABSTRACT

In our companion paper, we described the preparation and intercalation of two homologous series of dicarbonyl compounds, methyl *n*-oxooctadecanoates and the corresponding *n*-oxooctadecanoic acids (*n* = 4–16), into DMPC liposomes. ^{13}C NMR chemical shift of the various carbonyls was analyzed using an $E_T(30)$ solvent polarity–chemical shift correlation table and the corresponding calculated penetration depth (in Å). An iterative best fit analysis of the data points revealed an exponential correlation between $E_T(30)$ micropolarity and the penetration depth (in Å) into the liposomal bilayer. However, this study is still incomplete, since the plot lacks data points in the important area of moderately polarity, i.e., in the E_T (30) range of 51–45.5 kcal/mol. To correct this lacuna, a family of ketophospholipids was prepared in which the above *n*-oxooctadecanoic acids were attached to the *sn*-2 position of a phosphatidylcholine with a palmitic acid chain at *sn*-1. To assist in assignment and detection several derivatives were prepared ^{13}C-enriched in both carbonyls. The various homologs were intercalated into DMPC liposomes and give points specifically in the missing area of the previous polarity–penetration correlation graph. Interestingly, the calculated exponential relationship of the complete graph was essentially the same as that calculated in the companion paper based on the methyl *n*-oxooctadecanoates and the corresponding *n*-oxooctadecanoic acids alone. The polarity at the midplane of such DMPC systems is ca. 33 kcal/mol and is not expected to change very much if we extend the lipid chains. This paper concludes with a chemical ruler that maps the changing polarity experienced by an intercalant as it penetrates the liposomal bilayer.

1. Introduction

Because of our work on the organic reactions of active oxygen species, we have been interested in determining the depth (i.e., the distance from the water–lipid interface) of substrates intercalated (dubbed intercalants) within the lipid bilayer of liposomes and biological membranes. To accomplish this, it was first necessary to conjoin two observations. The first is that lipid bilayers contain a polarity gradient stretching from the highly polar lipid–aqueous interface, down to the non-polar lipid slab. The second is the generally excellent correlation between the ^{13}C NMR chemical shift (δ) of polarizable moieties (like C=O and P=O) with solvent polarity (using the Dimroth–Reichardt $E_T(30)$ polarity parameter) (Reichardt, 1965, 1994; Reichardt and Welton, 2011). Once a $\delta/E_T(30)$ correlation graph has been prepared, the chemical shift of an intercalated polarizable group reflects the micropolarity it experiences. From this we can qualitatively surmise the location of the polar moiety and, hence, the intercalant's depth within the bilayer (Frimer et al., 1996; Afri et al., 2002; Afri et al., 2004a,b; Bodner et al., 2010; Cohen et al., 2008a,b,c; Shachan-Tov et al., 2010).

The next stage in this project was to prepare a "chemical ruler" which would allow one to convert the qualitative $E_T(30)$ depth numbers to the corresponding quantitative Angstrom values. In the companion paper (Afri et al., 2014), we outlined the synthesis of two homologous series of bifunctional molecules: ketoesters **1** and ketoacids **2** (Fig. 1). Ketoesters **1** and ketoacids **2** were intercalated into the liposomal bilayer in the hope of mapping the polarity

* Corresponding author at: The Ethel and David Resnick Chair in Active Oxygen Chemistry, The Department of Chemistry, Bar-Ilan University, Ramat Gan 5290002, Israel. Tel.: +972 3 5318610; fax: +972 3 7384053.
E-mail addresses: Michal.Afri@biu.ac.il (M. Afri), C_Eliasi@walla.com (C. Alexenberg), Pinchas.Aped@biu.ac.il (P. Aped), Efrat.Bodner@biu.ac.il (E. Bodner), SaritCohen84@gmail.com (S. Cohen), MichalDomb@gmail.com (M. Ejgenberg), ShlomiEliyohu@gmail.com (S. Eliyahu), Pessia.Sharon@biu.ac.il (P. Gilinsky-Sharon), IfatAsh@Yahoo.com (Y. Harel), MiriamNaqqash@gmail.com (M.E. Naqqash), HaniPorat@gmail.com (H. Porat), Ayala.Ranz@gmail.com (A. Ranz), Aryeh.Frimer@biu.ac.il (A.A. Frimer).

http://dx.doi.org/10.1016/j.chemphyslip.2014.07.003
0009-3084/

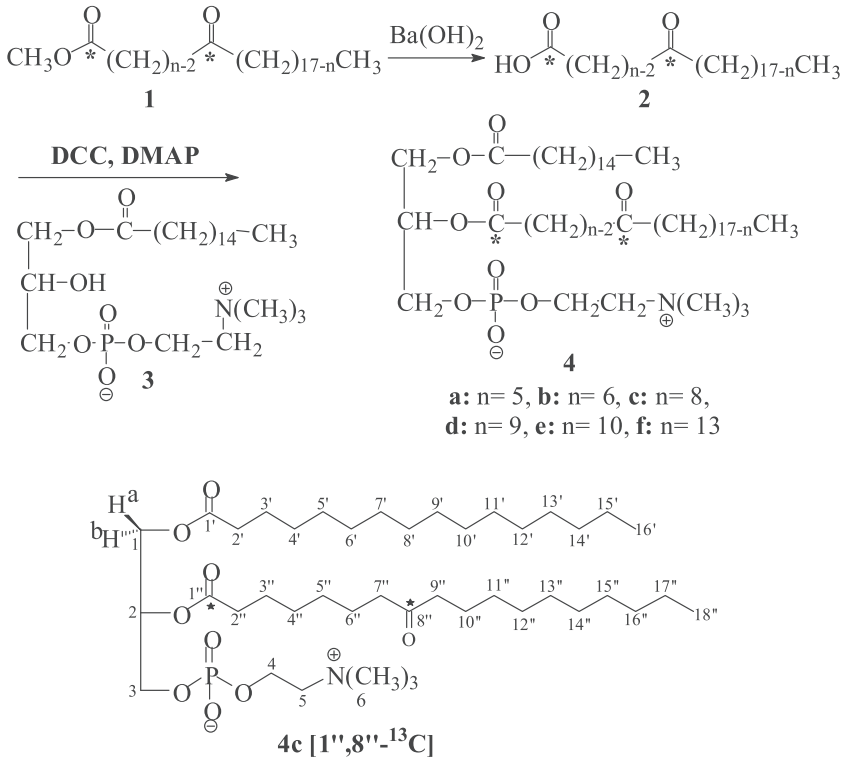

Fig. 1. General synthesis for ketophospholipids **4**.

changes along the whole length of the DMPC bilayer. The results surprisingly revealed that the head groups (C-1) in each case were not anchored near the water layer, as is often assumed – especially for the fatty acids. Furthermore, the head groups in each family do not even lie at the same depth for all the derivatives. Nevertheless, an iterative best fit analysis of the data points obtained allowed us to obtain an exponential curve, which gives us substantial insight into the correlation between $E_T(30)$ micropolarity and penetration depth into the liposomal bilayer. Lacking still for our curve are data points in the $E_T(30)$ range of 51–45.5 kcal/mol.

In the present paper we describe the synthesis of the ketophospholipids (ketoPC) **4a-f**, by coupling ketoacids **2** with lysophosphatidylcholine **3** (Fig. 1), according to the procedure Menger et al. (1989). To assist in assignment and detection several derivatives were prepared ^{13}C-enriched in both carbonyls. The numbering of the various carbons is exemplified at the bottom of Fig. 1 for the doubly ^{13}C-labeled 8″-oxo derivative **4c**. For convenience, the names of the compounds were abbreviated as "*n*-ketoPC", where "*n*" signifies the location of the oxo group along the C-2 ester chain. Thus 8″-oxo derivative **4c** is dubbed 8-ketoPC. The various ketoPCs were then intercalated within DMPC liposomes. Because of the highly polar phosphatidylcholine head group, we fully expected each ketoPC derivative to be anchored in the polar region of the liposomal bilayer. Furthermore, from our previous work (Cohen et al., 2008a), we knew that the two glycerol ester carbonyls of DMPC in the liposome are situated at a polarity of ca. 50–52 kcal/mol. This led us to believe that the ester carbonyls of ketoPCs **4a-f** would fall in the desired 51–45 kcal/mol region. Using the NMR method described briefly above and in more detail in the companion paper (Afri et al., 2014), we hoped to determine the $E_T(30)$ polarity sensed by the various ester and ketone carbonyls in these ketoPCs. Combining these qualitative polarity results with the quantitive angstrom distance between the ketone and the ester carbons should allow us to complete the preparation of the desired ruler.

Table 1
^1H NMR data for compounds **4a-f**. (Missing entries are identical to the value of the last entry above them.)

	4a	4b	4c	4d	4e	4f
H-1a	4.12	4.14	4.12	4.12	4.12	4.10
H-1b	4.38	4.39	4.42	4.38	4.39	4.36
H-2	5.20	5.21	5.19	5.19	5.19	5.17
H-3	3.96	4.01	4.05	3.93	3.95	3.89
H-4	4.31	4.33	4.30	4.32	4.30	4.28
H-5	3.79	3.97	3.87	3.80	3.81	3.78
H-6	3.35	3.38	3.37	3.34	3.67	3.33
H-2′	2.27	2.28	2.29[b]	2.27	2.30[b]	2.25
H-3′	1.54	1.57	1.55	1.55	1.56	1.55
H-4′–H-15′	1.25	1.26	1.26	1.25	1.26	1.23
H-16′	0.88	0.88	0.88	0.88	0.88	0.86[b]
H-2″	2.32	2.32	2.27[b]	2.30	2.27[b]	2.27
H-3″	1.84	1.57	1.55	1.55	1.56	1.55
H-4″	2.47	1.57	1.26	1.25	1.26	1.23
H-5″	–[a]	2.42				
H-6″	2.38	–[a]	1.55			
H-7″	1.54	2.40	2.39[c]	1.55		
H-8″	1.25	1.57	–[a]	2.38	1.56	
H-9″		1.26	2.38[c]	–[a]	2.38	
H-10″			1.55	2.37	–[a]	
H-11″			1.26	1.55	2.38	1.55
H-12″				1.25	1.56	2.36
H-13″					1.26	–[a]
H-14″						2.36
H-15″						1.55
H-16″						1.23
H-17″						
H-18″	0.88	0.88	0.88	0.88	0.88	0.87[b]

[a] Carbonyl position.
[b] The assignments for these absorptions are indefinite and may be interchangeable with each other.
[c] The assignments for these absorptions are indefinite and may be interchangeable with each other.

Table 2
^{13}C NMR data for compounds **4a-f**. (Missing entries are identical to the value of the last entry above them.)

	4a	4b	4c	4d	4e	4f
C-1	62.8	62.11	63.02	62.92	62.99	62.1
C-2	70.81	70.42	70.69	70.42	70.61	70.42
C-3	63.59	63.4	63.54	63.55	63.45	63.62
C-4	59.32	58.97	66.45	59.44	66.39	66.48
C-5	66.39	65.96	59.41	66.25	59.45	59.43
C-6	54.46	53.94	54.45	54.36	54.41	54.5
C-1′	173.59[a]	173.43[a]	173.64	173.60[a]	173.53	173.68[a]
C-2′	34.02[b]	34.12[b]	34.27[a]	34.22[b]	34.32[a]	34.44[b]
C-3′	24.87	24.92c	24.98	24.86[c]	24.94	25.10[c]
C-4′–C-13′	29.74	29.76	29.81	29.75	29.76	29.86
	29.72	29.70	29.66	29.69	29.61	29.69
	29.71	29.57	29.59	29.61	29.41[b]	29.61
	29.68	29.50[d]	29.53[b]	29.46		29.50[d]
	29.58[b]			29.39		
				29.29[d]		
C-14′	31.94	31.94	32.01[c]	31.94[e]	31.96[c]	32.05[c]
C-15′	22.71	22.71	22.76	22.71[f]	22.72[d]	22.81[e]
C-16′	14.14	14.13	14.19	14.14[g]	14.14[e]	14.23[f]
C-1″	172.63[a]	172.80[a]	173.16	173.19[a]	173.13	173.34[a]
C-2″	33.36[b]	34.06[b]	34.20[a]	34.11[b]	34.17[a]	34.25[b]
C-3″	18.85	24.41[c]	24.8	24.79[c]	24.94	25.02[c]
C-4″	42.95[c]	23.92[e]	29.45[b]	29.23	29.32	29.44
C-5″	210.61	42.45[f]		29.18[d]	29.19[b]	29.35
C-6″	41.33[c]	211.78	23.98[d]			
C-7″	23.86	41.90[f]	42.98[e]	23.89[e]		
C-8″	29.49	23.09[e]	211.48	42.87[h]	23.93[f]	
	29.38					
	29.30					
	29.20[b]					
C-9″		29.39	42.70[e]	21.53	42.88[g]	
		29.35				
		29.25[e]				
C-10″			23.67[d]	42.71[h]	211.5	
C-11″			29.39	23.75[e]	42.73[g]	24.68[g]
			29.28			
			28.99[b]			
C-12″				29.12	23.85[f]	42.93[h]
				29.00		
				28.94[d]		
C-13″					29.11[b]	211.72
C-14″						42.89[h]
C-15″						23.68[g]
C-16″	31.94	31.94	31.98[c]	31.88[e]	31.86[c]	31.57[c]
C-17″	22.71	22.71	22.76	22.68[f]	22.67[d]	22.58[e]
C-18″	14.14	14.13	14.19	14.13[g]	14.11[e]	14.04[f]

[a–h]The assignments for these absorptions are indefinite and may be interchangeable with each other.

2. Materials and methods

2.1. General

Nuclear magnetic resonance (NMR) spectra were recorded on a variety of Bruker Fourier transform spectrometers: DRX 200 MHz, DRX 300 MHz, DMX 600 MHz or Avance III 700 MHz. For 1D NMR spectra, a QNP probe was used. All 2D experiments (COSY, HMQC, HMBC, and NOSEY) were run and processed by Bruker software. NMR spectra were generally run at 25 ± 1 °C except in the case of DMPC liposomes, which were run at physiological temperature 37 ± 1 °C, above the phase transition temperature (T_m) of DMPC which is 23.6 °C (Sassaroli et al., 1990). ^{1}H and ^{13}C NMR chemical shifts are expressed in δ (ppm) relative to tetramethylsilane (TMS; 0 ppm). Generally the sample was calibrated by internal TMS, though sometimes relative to the solvent. In the case of aqueous vesicle solutions, we calibrated the spectrum according to the trimethylammonium peak at 54.6 ppm. In the ^{13}C NMR spectra of the long chain derivatives, there are chemical shifts which overlap; hence, the number of chemical shifts does not always match the number of carbons. We also note that in the hydrogen and carbon assignments below, the carbons were generally numbered to be consistent with the rules of nomenclature. The designation "*t*" or "quint" indicates a triplet or quintet with second order coupling or broadening.

Mass spectra (MS) and high resolution mass spectra (HRMS) were collected in an AutoSpec Premier manufactured by Waters (UK) in DCI/CH_4 or CI/CH_4 mode, or in Q TOF manufactured by Waters (UK) in ESI mode. MALDI mass spectra were obtained on Autoflex III TOF/TOF, manufactured by Bruker (Germany). Infra-red Fourier transform spectra (FTIR) were obtained using a Bruker Vector 22 instrument, with the data processed by Opus 5.0 (Bruker) software. The spectra were analyzed with IR MentorPro 6.5 (Bio-Rad) software. Abbreviations used for reporting % transmittance were: s = strong (100 – 75%), m = medium (75–45%), w = weak (45–25%), v = very and b = broad. Melting points were run on a Uni-Melt Thomas Hoover-capillary melting point apparatus manufactured by Thomas (Philadelphia PA, USA). Sonications were carried out using a probe sonicator [Vibra-Cell™ VCX130 Sonics and Materials Inc., ultrasonic processor with 20 kHz output frequency and a titanium alloy Ti-6Al-4V probe]. Other standard equipment included a Winn Vortex Genie.

2.2. Chemicals

N,*N*′-Dicyclohexylcarbodiimide (DCC), 4-dimethylaminopyridine (DMAP), dimyristoyl phosphatidylcholine (DMPC), and the deuterated solvents were obtained from Sigma–Aldrich. 1-Palmitoyl-2-hydroxy-*sn*-glycero-3-phosphatidylcholine (**3,** LysoPC) was purchased from Avanti Polar Lipids, Alabaster, Germany. Phosphate buffer saline solution pH 7.4 (PBS-N_3) was prepared using doubly distilled water (dd H_2O – purified via Millipore Milli-Q columns) containing 1.7 mM NaH_2PO_4, 8.1 mM Na_2HPO_4, 2.7 mM KCl, 137 mM NaCl and 1 wt% sodium azide.

2.3. Sonic intercalation of compounds into DMPC liposomal solutions

The general procedure for the preparation of sonically intercalated DMPC liposomal suspensions for the NMR studies has been described in the companion paper (Afri et al., 2014). Generally speaking, the intercalant concentration within the liposomal solution is 0.05 M and the ketoPC:DMPC molar ratio is 1:4.

2.4. General procedure for the preparation of 1-palmitoyl-2-(n″-oxostearoyl)-sn-glycero-3-phosphatidylcholine **4**

As outlined in Fig. 1, ketophospholipids **4** were prepared by coupling ketoacids **2** with lysoPC **3** according to the procedure of Menger et al. (1989). Ketoacids **2** were prepared, in turn, from ketoesters **1** as described in the companion paper (Afri et al., 2014). To assist in assignment and detection, several derivatives were prepared which were ^{13}C-enriched in both carbonyls by coupling the lysoPC **3** with doubly labeled ketoacids **2**. The NMR spectral data and assignments appear in Tables 1 and 2, while the complete spectral data including integration and splitting constants appear in the Supplementary Information.

2.4.1. 1-Palmitoyl-2-(5″-oxostearoyl)-sn-glycero-3-phosphatidylcholine (5-ketoPC, ***4a***)

46% yield, mp 86 °C. MS (MALDI matrix DHB) *m*/*z* 776.659 (M^+). FTIR 2971 (s), 2956 (s), 2882 (m), 1750, 1737 and 1699 (m, C═O) 1542 (m), 1508 (m), 1457 (m), 1247, 1130 and 1128 (m, C—O and P═O), 835 (w, P—O—R-ester) cm^{-1}.

2.4.2. 1-Palmitoyl-2-(6″-oxostearoyl)-sn-*glycero-3-phosphatidylcholine (6-ketoPC, **4b**)*

32% yield, mp 92 °C. MS (MALDI matrix DHB) *m/z* 776.847 (M^+). FTIR 2962 (s), 2930 (s), 2876 (m), 1749, 1733 and 1715 (m, C=O) 1540 (s), 1507 (m), 1457 (m), 1117 and 1110 (m, C—O and P=O), 851 (w, P—O—R-ester) cm^{-1}.

2.4.3. 1-Palmitoyl-2-(8″-oxostearoyl)-sn-*glycero-3-phosphatidylcholine (8-ketoPC, **4c**)*

38% yield, mp: 81 °C. MS (MALDI matrix DHB) *m/z*: 776.837 (M^+). FTIR: 2994, 2946 (s), 2891 (m), 1717 (vbr w, C=O), 1541 (w), 1221, 1105 (w, C—O, P=O), 865 (w, P—O—R) cm^{-1}.

2.4.4. 1-Palmitoyl-2-(1″,8″-^{13}C-8″-oxostearoyl)-sn-*glycero-3-phosphatidylcholine (^{13}C-8-ketoPC, ^{13}C-**4c**)*

35% yield. MS (TOF ES^-) *m/z* 776 (M^+, 100%).

2.4.5. 1-Palmitoyl-2-(9″-oxostearoyl)-sn-*glycero-3-phosphatidylcholine (9-ketoPC, **4d**)*

28% yield. MS (TOF ES^-) *m/z* 776 (M^+, 100%).

2.4.6. 1-Palmitoyl-2-(10″-oxostearoyl)-sn-*glycero-3-phosphatidylcholine (10-ketoPC, **4e**)*

39% yield, mp: 80 °C. MS (MALDI matrix DHB) *m/z*: 776.588 (M^+). FTIR: 2968, 2938 (s), 2881 (m), 1717, 1653 (w, C = O), 1540, 1457 (w), 1211, 1209 (w, C—O, P=O), 866 (w, P—O—R) cm^{-1}.

2.4.7. 1-Palmitoyl-2-(13″-oxostearoyl)-sn-*glycero-3-phosphatidylcholine (13-ketoPC, **4f**)*

40% yield. MS (TOF ES^-) *m/z* 776 (M^+, 100%).

2.5. NMR conditions for preparing correlation graphs and liposomal samples

For the correlation graph, samples (ca. 10 mg) of ketoPCs **4** were dissolved in 0.6 mL of pure solvent to give a final concentration of 0.05 M. This is approximately the same concentration as that of the intercalants within the liposomal solution. The samples in pure solvents were scanned for 20 min. or 1000 scans. Liposomal samples were prepared as described above in sec. 2.3 and were scanned overnight (40,000 scans). D_2O served as the internal lock.

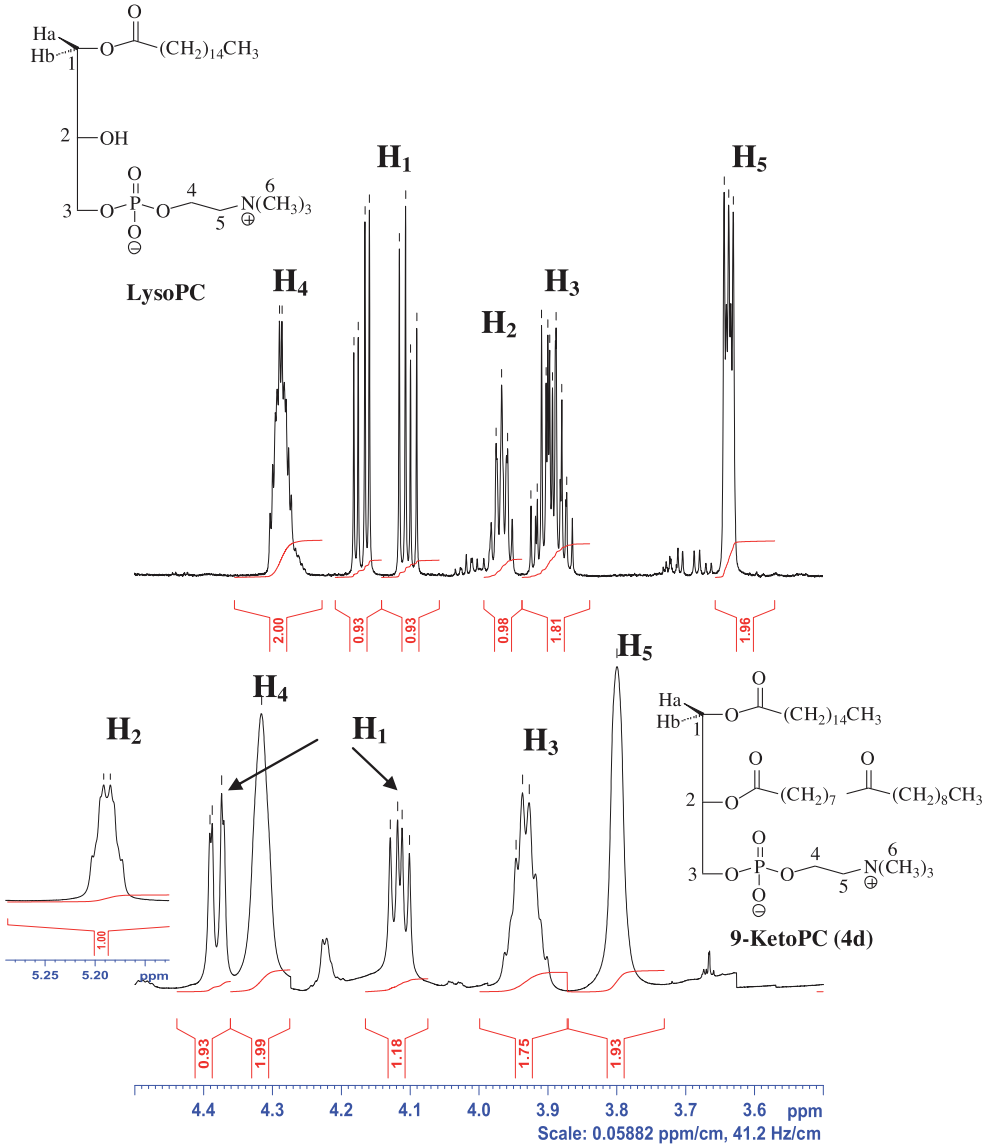

Fig. 2. Comparison of the ^{1}H NMR spectra of lysoPC (**3**) and 9-ketoPC (**4d**).

3. Results and discussion

3.1. General synthesis of ketophospholipids **4**

As mentioned in our introductory comments, our main goal was to synthesize a family of phospholipids **4**, having keto-groups at various locations along the fatty-acid chain. Ketoesters **1** and ketoacids **2** were prepared as described in the companion paper (Afri et al., 2014). Following the Menger approach (Menger et al., 1989), the ketoacids were then coupled with 1-palmitoyl-2-hydroxy-*sn*-glycero-3-phosphatidylcholine (lysoPC **3**), mediated by DCC and DMAP, to give the corresponding 1-palmitoyl-2-(*n*″-oxostearoyl)-*sn*-glycero-3-phosphatidylcholines **4** in yields of ca. 40%. The ^{1}H and ^{13}C NMR spectral data of compounds **4** appear in Tables 1 and 2. These compounds are quite intriguing from an NMR spectral perspective and their identification involved not only standard ^{1}H and ^{13}C NMR analysis but also a variety of 2D-NMR techniques. This analysis further allowed us to readily distinguish between the ketophospholipid products and the lysoPC starting material. The details of this analysis appear in the next section.

3.2. Identification of ketophospholipid products by NMR

The formation of ketoPCs **4** from lysoPC **3** was most easily verified by the chemical shift of the methylene protons H_1–H_5 in the ^{1}H NMR spectrum, as exemplified by 9-ketoPC **4 d** in Fig. 2. The most dramatic change occurs in H_2, which moves downfield by approximately 1.25 ppm in this transformation. This is because carbon C_2 goes from being adjacent to a hydroxyl group (a quintet at 3.95) in the starting material, to being α to an ester moiety (multiplet at ca. 5.2 ppm) in the product. At the same time, one can detect a small concomintant upfield movement in H_3–H_5. The

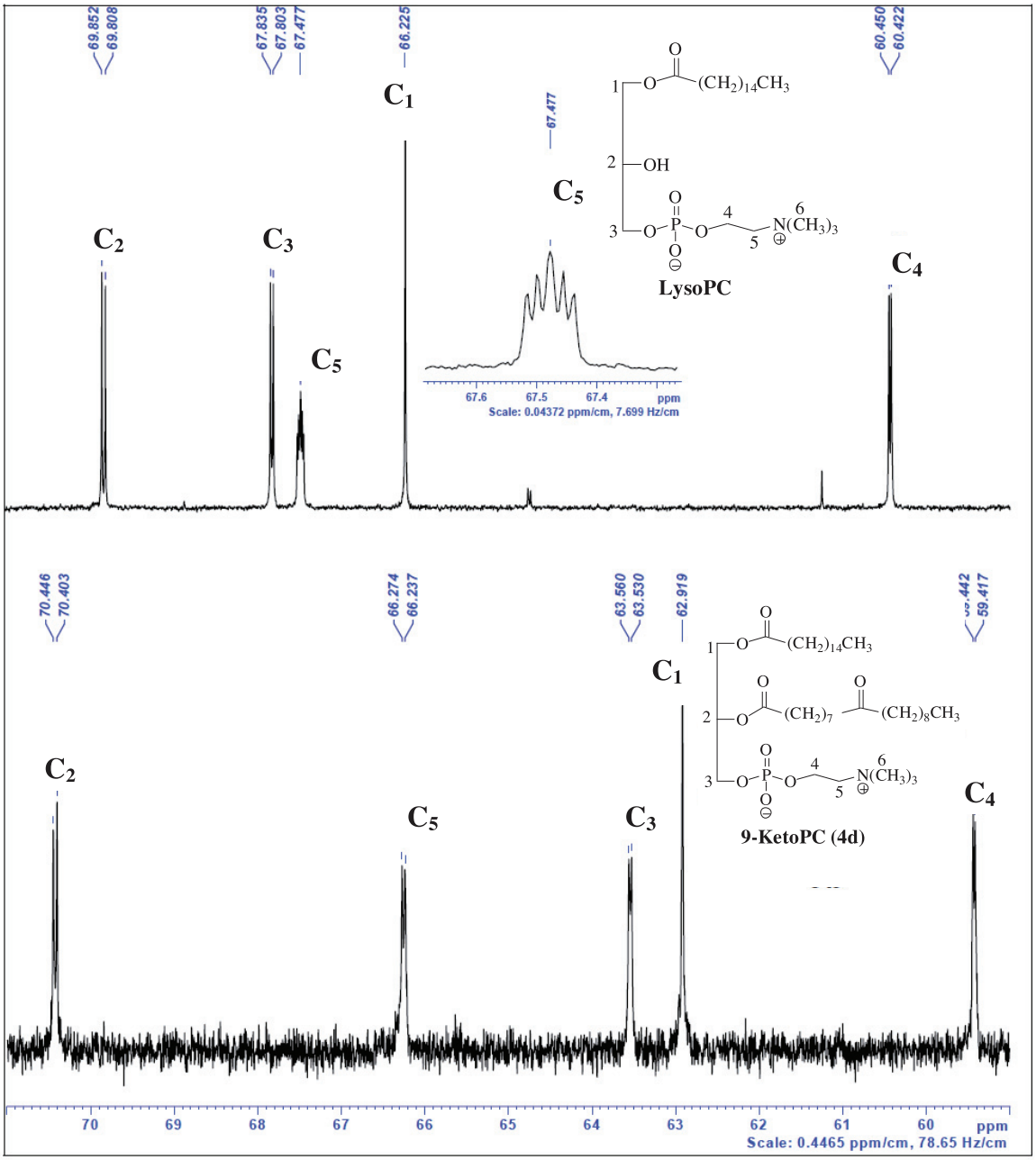

Fig. 3. Comparison of the ^{13}C NMR spectrums of lysoPC (**3**) and 9-ketoPC (**4d**).

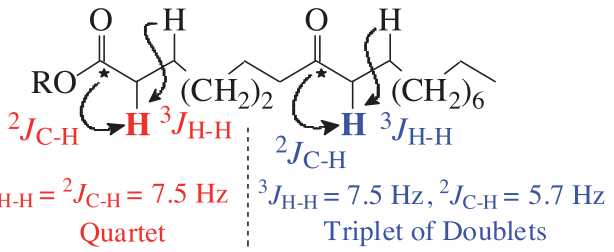

Fig. 4. Coupling constants and splitting in ^{1}H NMR of ^{13}C enriched phospholipid **4d-13C**.

diasteriotopic protons H_{1a} and H_{1b} appear, respectively, at 4.12 and 4.18 ppm in lysoPC **3,** but at ca. 4.1 and 4.4 ppm in ketoPCs **4**.

Turning now to ^{13}C NMR spectroscopy, carbons C_1–C_5 of lysoPC **3** and ketoPC **4** are quite different, as shown in Fig. 3. Esterification of the hydroxyl group engenders both β and γ effects. In the case of C_2 these effects essentially cancel each other out with a slight net downfield shift of ca. 0.5 ppm. The larger upfield movements (ca 4 ppm) of C_1 and C_3 result from a γ-effect of the ester carbonyl on these carbons.

We also note that in both lysoPC **3** and ketoPC **4**, the carbons (C_2–C_5) which lie two or three atoms from the phosphorous atom are split into doublets by ^{31}P ($I = 1/2$). Interestingly, however, only in lysoPC does C_5 appear as a quintet (see the enlargement in Fig. 3). This is in fact a doublet of triplets with overlapping lines which results from splitting by ^{31}P ($I = 1/2$) into a doublet ($J_{PC} = 6$ Hz), and by ^{14}N ($I = 1$) into a 1:1:1 triplet ($J_{CN} = 3$ Hz). The uncommon ^{14}N splitting is known in quaternary ammonium salts with high tetrahedral symmetry. Nevertheless, this phenomenon does not appear in the ketoPCs, apparently because slight changes in a compound's symmetry has a dramatic effect on the size and shape of the ^{14}N splitting pattern (Ogg and Ray, 1957).

3.3. Identification of ^{13}C-enriched ketophospholipid products by NMR

We also synthesized the doubly ^{13}C-labeled 8-ketoPC (**13C-4c**) enriched in both the C_1-ester and C_8-ketone carbonyls of the C2 fatty acid chain. The resulting NMR spectrum of this labeled compound is more complicated because of the additional $J_{C-C'}$ J_{C-H} and J_{H-H} splittings. Thus, $H_{2''}$ in the unlabeled **4c** falls at 2.29 ppm and is split into a triplet by the adjacent C_3 methylene ($J_{H2-H3} = 7.5$ Hz) (see Figs. 4 and 5). [This triplet overlaps with a similar $H_{2'}$ triplet at 2.27 ppm corresponding to the methylene α to the C_1-ester]. In the labeled analog **13C-4c**, $H_{2''}$ is now also split by the adjacent labeled C_1-ester carbonyl carbon. This should have given us a triplet of doublets pattern, but instead a quartet is observed. This is simply because the two bond C–H splitting ($^{2}J_{C1-H2}$) is of the same size (7.5 Hz) as the three bond vicinal H–H coupling ($^{3}J_{H2-H3}$). [Resolution enhancement allowed us to distinguish between this quartet and the abovementioned $H_{2'}$ triplet (see Figs. 4 and 6).]

We turn now to $H_{7''}$ and $H_{9''}$ methylenes straddling the C_8 ketone of **4c**. In the unlabeled analog they fall together at 2.38 ppm as a 4H triplet ($J_{HH} = 7.5$ Hz) (see Figs. 4 and 5). In the labeled analog, however, resolution enhancement reveals that these triplets are further split by the adjacent labeled ketone carbonyl carbon at C_8 ($^{2}J_{C-H} = 5.7$ Hz), yielding triplet of doublets (see Figs. 4 and 6).

3.4. Preparation of the correlation graphs and calculating $E_T(30)$ within DMPC liposomes.

As mentioned in the Introduction, we were interested in quantitatively determining the depth and orientation of substrates intercalated within the liposomal bilayer. In order to do so, we synthesized a family of ketophospholipids **4**, each member containing three carbonyls – two glycerol esters and a ketone. For each molecule, the chemical shifts of the ketone and two ester carbonyls in solvents of various polarities [$E_T(30)$ in kcal/mol (Reichardt, 1994)] were measured. A ^{13}C NMR chemical shift–polarity correlation graph was created for each compound. The correlation graphs make it possible to measure the polarity of the microenvironment of a specific carbonyl and its qualitative depth within the liposome.

The amphiphilicity of the ketoPCs caused some solubility problems. Thus, the non-protic moderately polar solvents acetone ($E_T(30) = 42.2$ kcal/mol) and acetonitrile (45.6) did not dissolve the phospholipid derivatives at all, while benzene (34.3) dissolved only some of the keto-PCs. After much testing, we found that one

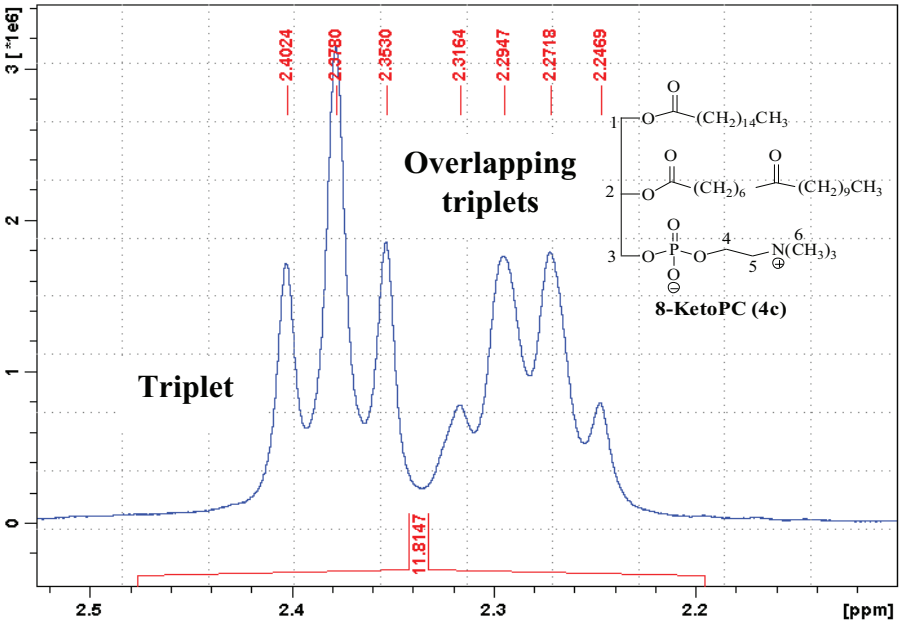

Fig. 5. Expansion of ^{1}H NMR of 8-ketoPC **4c** showing the hydrogens α to the ester and ketone.

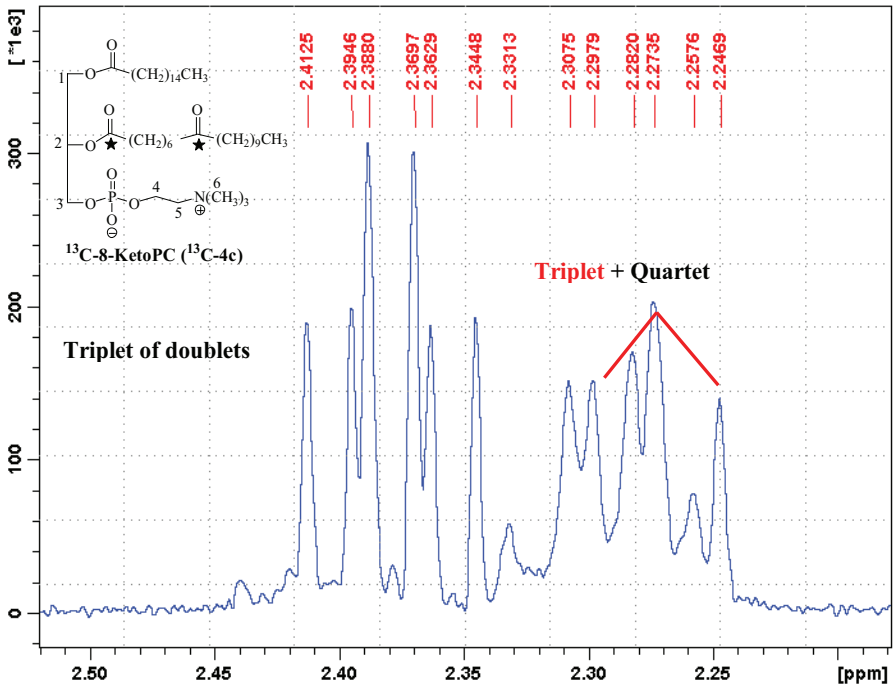

Fig. 6. Expansion of ^{1}H NMR of 8-ketoPC **13C-4c** showing the hydrogens α to the ester and ketone.

aprotic and five protic solvents, in a broad range of polarity values, did indeed dissolve ketoPCs **4** sufficiently to allow for a measurement of the ^{13}C NMR of these molecules. These solvents included methanol ($E_T(30)$ = 55.5 kcal/mol from Reichardt (1994)), ethanol (51.9), *i*-propanol (48.4), *t*-butanol (43.3), 2-methyl-2-butanol (2-Me-2BuOH) (41.0) and tetrachloromethane (32.4). The correlation graph had a good correlation coefficient ($r^2 > 0.9$).

The next stage was to intercalate the ketoPCs **4** within the DMPC liposomal bilayer. Generally speaking, when we intercalate various substrates within liposomes we are careful to use an intercalant: DMPC ratio of 1:5. We do this so as not to dramatically change the physical properties of the liposomal host. In the present experiments, however, the intercalant itself is a phospholipid, with the keto group present on only one of the two fatty acid chains. This allowed us to increase the relative amount of the ketoPCs intercalated resuting in a ketoPC:DMPC ratio of 1:4, with little concern about any significant change in the liposomal structure. This is because the amount of keto group actually present is still effectively close to a 1:5 ratio. Thus, in the present experiments the ketoPC:DMPC ratio was 1:4, which permitted more facile identification of the keto-carbonyl of **4**. The ketoPC concentration in the samples was 0.05 M. We should note that the ^{13}C chemical shifts of the C-1 ester carbons of DMPC and those of the ketoPCs are very similar. Use of ^{13}C-enriched analogs aided us in determining that the broad shaped signals belong to DMPC, while the sharp peaks result from the ester of the ketoPCs.

We will exemplify our results by focusing on 8-ketoPC **4c**. Table 3 lists ^{13}C NMR chemical shifts of ketone C8, and esters C-1′ and C-1″ in various solvents and within DMPC liposomes. Fig. 7 plots these chemical shifts as a function of solvents polarity revealing that, as expected, the chemical shift values increase with solvent polarity. The correlations were excellent with correlation coefficients (R^2) of 0.96–0.97. The line equations of the correlation graphs allowed us to calculated the $E_T(30)$ value experienced by the carbonyls of ketone C8, and esters C-1′ and C-1″ within the liposomal bilayer, which appear at the bottom of Table 3.

The same procedure was applied to all the members of the ketoPC series **4**. Table 4 summarizes the calculated $E_T(30)$ values for the various carbonyls in these ketoPC derivatives intercalated within DMPC liposomes. For purposes of comparison, this table also includes the calculated $E_T(30)$ value of the DMPC ester carbonyls C-1′ and C-1″ within DMPC liposomes. We should note that the chemical shifts for the C-1′ and C-1″ ester carbonyls are similar, but not identical. (The ^{13}C enriched C-1″ carbon of the labeled analogs aided us in distinguishing between the two esters.) As a rule, the C-1″ carbonyl resides at a higher polarity (ca. 50.5 kcal/mol) than the corresponding C-1′ ester (ca. 47.5 kcal/mol). This reflects the fact that as compared to

Table 3
^{13}C NMR chemical shifts of 1-palmitoyl-2-(8″-oxostearoyl)-*sn*-glycero-3-phosphatidylcholine (**4c**) in various solvents and within DMPC liposomes.

Solvent	$E_T(30)$ (kcal/mol)	δ of C8 ketone (ppm)	δ of ester C-1′ (ppm)	δ of ester C-1″ (ppm)
CCl_4	32.4	207.07	171.58	171.58
2-Me-2-BuOH	41.0	209.65	172.95	172.30
t-BuOH	43.3	211.02	173.40	173.03
i-PrOH	48.4	211.53	173.58	173.20
EtOH	51.9	212.28	174.02	173.65
MeOH	55.5	213.54	174.80	174.40
R^2		0.97	0.96	0.96
DMPC liposome (calc. $E_T(30)$)		209.78 (41.4)	173.79 (48.5)	173.71 (51.2)

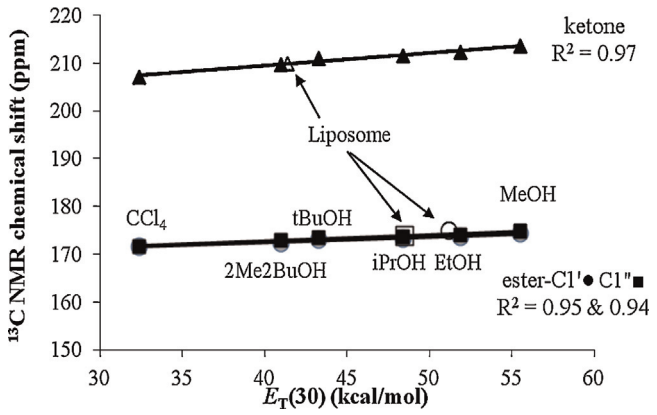

Fig. 7. Correlation graph of 1-palmitoyl-2-(8″-oxostearoyl)-*sn*-glycero-3-phosphatidylcholine (**4c**).

C-1′, the C-1″ carbonyls lie on the upper glycerol carbon nearer to the phosphate headgroup, and hence is slightly higher in the bilayer. Thus, the polar head groups for all derivatives of **4** are indeed anchored in the polar region of the bilayer not far from the interface. Also, as expected, the calculated $E_T(30)$ values of the ketones decrease as it moves down the lipid chain. For example, ketone C-5″ in **4a** senses a polarity of E_T = 43.4 kcal/mol while C-13″ (**4f**) is located substantially deeper in the bilayer at E_T = 34.4 kcal/mol.

3.5. The change in $E_T(30)$ as a function of penetration depth (PD) of ketoPCs **4**

For the purpose of constructing a molecular ruler, it is imperative to determine how the $E_T(30)$ value changes as function of the penetration depth (PD in Å) within the liposome. As described in the companion paper (Afri et al., 2014), we used data obtained from ketoesters **1** and ketoacid **2,** together with an iterative best fit analysis to obtain an exponential curve. This curve assumes that the starting point for DMPC liposomal penetration (PD = 0 Å) is the edge of the polar choline head group, namely, at the top of the water–lipid interface. The $E_T(30)$ polarity at this point is that of water, 63 kcal/mol (Reichardt, 1994). This exponential curve gives us two mathematical relationships between PD and the corresponding $E_T(30)$ value, as shown in Eqs. (1) and (2):

$$E_T(30) = 31.5 + 31.5 \times \exp(-0.137\mathrm{PD}) \quad (1)$$

$$\mathrm{PD} = 7.30 \times \ln\frac{31.5}{(E_T(30) - 31.5)} \quad (2)$$

We note that from a practical perspective, using Eq. (2) to calculate the PD values from the corresponding $E_T(30)$ numbers works well (i.e., gives good results with only small errors) only in the more polar area of the bilayer [$E_T(30) \gtrsim 37$]. However, as we move to the very lipophilic areas of the liposomal bilayer, a slight error in E_T leads to a very large error in the calculated PD. As a result, a more reliable means for determining the PD of C-*n*″, is to calculate the PD of the headgroup C-1″ using Eq. (2), and then adding to it the PCMODEL calculated distance from C-1″ to C-*n*″, $\Delta d(\text{C-1} - \text{C-}n'')_{\mathrm{Calc}}$. This in effect is Eq. (3).

$$\mathrm{PD\,C-n''} = \mathrm{PDC-n''} + \Delta d(\mathrm{C-l''-C-n''}) \quad (3)$$

(The applicability of PCMODEL MMX calculations for measuring distances in these long-chain systems is discussed in the companion paper (Afri et al., 2014).

As pointed out in the Introduction, despite the above success in correlating $E_T(30)$ polarity with penetration depth, the correlation Eqs. (1) and (2) were based on data lacking points in the important $E_T(30)$ range of 51–45 kcal/mol. However, this missing information can now be gleaned from Table 4 for ketoPCs **4,** described in the previous section. What is necessary, then, is to add the new data points for **4** to the graph already obtained in the companion paper for ketoesters **1** and ketoacid **2**.

This we accomplished as follows: the ester carbonyls (C-1″) of **4a-f** were placed on the curve described by Eq. (1), according to their determined $E_T(30)$ values (see Table 4). The position of these points on the curve determines the corresponding penetration depth of C-1″ (PD C-1″). The tail group carbonyls were then placed on the graph based on their determined $E_T(30)$ values and approximate PD, assuming that the latter value is governed by Eq. (3), where Δd(C-1″–C-*n*″) is the PCMODEL calculated distance from C-1″ to C-*n*″ in Å, listed in Table 4. The curve drawing program was then asked to find the exponential curve that would give the "best fit" for all the points (from dicarbonyl compounds **1**, **2** and **4**). Once this was done, the C1″ head groups were then moved (slightly–see below) to the curve and the "best fit" process repeated. Clearly, a revision of the initial PD value of the C-1″ headgroup carbonyls had a concomitant effect on the location of the tailgroup carbonyls, based on Eq. (1). This process was repeated iteratively, until obtaining the best fit required no further corrections. The results of the iteration are shown in Fig. 8, while Table 5 lists the calculated PD of carbons C-1″ and C-*n*″ in ketoPCs **4**.

We should emphasize that the corrections required for adding ketoPCs **4** to the curve for the second and subsequent iterations were truly negligible. Indeed, as seen in Fig. 9, the "best fit" line for all the carbonyls in ketoesters **1**, ketoacids **2** and ketoPCs **4** was essentially identical to that obtained in the companion paper (Afri et al., 2014) based on the former dicarbonyl compounds alone. As a result, we are confident that Eq. (1) accurately describes the change in $E_T(30)$ polarity along the DMPC lipid bilayer – and is thus a solid basis upon which to build our chemical ruler.

3.6. Constructing a chemical ruler

As described above, Eq. (1) has now been shown to correspond well to the polarity gradient behavior of liposomes sensed by three dicarbonyl systems: ketoesters **1,** ketoacids **2** and ketoPCs **4**. For the convenience of the reader, we have translated the exponential

Table 4
Calculated $E_T(30)$ values of carbonyl carbons C-1′, C-1″ and C-*n*″ of ketoPCs **4a-f** intercalated within DMPC liposomes.

Cmpd (*n*)	$E_T(30)$ ester C-1′	$E_T(30)$ ester C-1″	$E_T(30)$ ketone C-*n*″	Δd(C-1 – C-*n*″)[a] (Å)
DMPC	48.9	50.4	–	–
4a (*n* = 5)	46.4	51.1	43.4	5.00
4b (*n* = 6)	46.6	50.1	42.7	6.25
4c (*n* = 8)	48.5	51.2	41.4	8.75
4d (*n* = 9)	48.8	51.4	39.0	10.00
4e (*n* = 10)	47.2	49.1	37.4	11.25
4f (*n* = 13)	47.6	50.9	34.4	15.00

[a] Calculated with PCMODEL 7.50.00 Software (Bloomington, Indiana) using an MMX force field.

Table 5
$E_T(30)$ value (kcal/mol) and calculated penetration depth (PD in Å) of carbons C-1″ and C-*n*″ of ketoPCs **4** intercalated within DMPC liposomes.

Cmpd (*n*)	$E_T(30)$ C-1″	PD C-1″	PD C-*n*″	$E_T(30)$ C-*n*″	
	Exp.[a]	Calc.[b]	Calc.[c]	Exp.[a]	Calc.[d]
4a (*n* = 5)	51.1	3.46	8.46	43.4	41.4
4b (*n* = 6)	50.1	3.85	10.10	42.7	39.4
4c (*n* = 8)	51.2	3.43	12.18	41.4	37.4
4d (*n* = 9)	51.4	3.35	13.35	39.0	36.6
4e (*n* = 10)	49.1	4.25	15.50	37.4	35.3
4f (*n* = 13)	50.9	3.54	18.54	34.4	34.0

[a] From Table 4.
[b] From Eq. (2), using $E_T(30)$ C-1″ .
[c] From Eq. (3), where PD C-1″ was calculated from Eq. (2).
[d] From Eq. (1). The standard deviation for 6 points is 2.6 kcal/mol.

mathematical relationship of Eq. (1) and Fig. 9 into Table 6, which correlates changes in the penetration depth of an intercalant with the corresponding $E_T(30)$ polarity of the microenvironment.

Table 6 makes it clear that, in the uppermost highly polar portion of the liposomal bilayer, there is a precipitous drop in polarity; thus, it takes only 4 Å to go 13 polarity units – from 63 kcal/mol down to just below 50 kcal/mol. Thereafter, this decrease slows such that it takes another 6 Å to drop a further 10 kcal/mol, to 39.5 kcal/mol. Penetration of an additional 10 Å takes us only to 33.5 kcal/mol. Since the length of a the DMPC lipid is 22 Å, Table 6 indicates that the minimal polarity in such systems is ca. 33 kcal/mol. This will not change very much if we would extend the lipid chains. The best-fit equation suggests that with longer lipids the polarity approaches 31.5 kcal/mol asymptotically.

Before drawing our molecular ruler, several points need to be emphasized.

(1) Firstly, we remind the reader that our ruler will be linear in angstroms, but the corresponding $E_T(30)$ scale will be exponential in nature following Eq. (1).
(2) The starting point for our liposomal ruler (PD = 0 Å) is the edge of the polar choline head group, at the top of the water–lipid interface. The $E_T(30)$ at this point is presumably that of water, 63 kcal/mol.
(3) Various molecular modeling studies (Matsudaira et al., 2000; Venable et al., 1993) place the phosphate group of phosphatidylcholines slightly below the choline nitrogen which lies at the interface. Previous ^{31}P NMR studies by Cohen et al. (2008b) have shown that the DMPC phosphate phosphorous lies not far below the choline at a micropolarity of 60 kcal/mol. Table 6 places this phosphate phosphorous at a PD of ~1 Å. It is noteworthy that this phosphate value is close to the neutron diffraction data of Wiener and White (1992) which places the phosphate group at a PD of ~2 Å.
(4) The abovementioned work of Wiener and White (Wiener and White, 1992) places the glycerol ester carbonyls at PD of ca. 6 Å. We have shown that the glycerol esters are not identically located. As seen from Table 5, the upper C-1″ glycerol esters of DMPC is located at 50.4 kcal/mol (PD 4 Å) while the C-1′ glycerol esters is located at 48.9 kcal/mol, or at ca. 4.5 Å – again not far from the Wiener and White value.
(5) Finally, according to PCMODEL MMX calculations (Cohen et al., 2008a), the distance between the choline interface and the end of the 14-carbon myristic chains of DMPC is about 22 Å, which according to Table 6 has an $E_T(30)$ value of around 33 kcal/mol. Note, however, that the intercalated ketoPCs **4** contain one 16-carbon stearic chain and another 18-carbon palmitic chain, and their calculated lengths are ca 24.5 and 27 Å respectively. We posit that the liposome structure is predominantly determined by the DMPC lipids which represent more than 83% (5/6) of the lipids present. The longer palmitic and stearic chains can arrange themselves in one of two ways. In the first, the tail carbons cross the midplane and penetrate the complementary half of the bilayer. In this lower region of the second half of the lipid layer, the $E_T(30)$ polarity is also expected to be ca. 33 kcal/mol. An alternative suggestion is that the long tails situate themselves in the midplane. This latter approach has been widely used to describe the location of the ubiquinone tails, or even rings, within the bilayer (reviewed by Afri et al., 2004a).

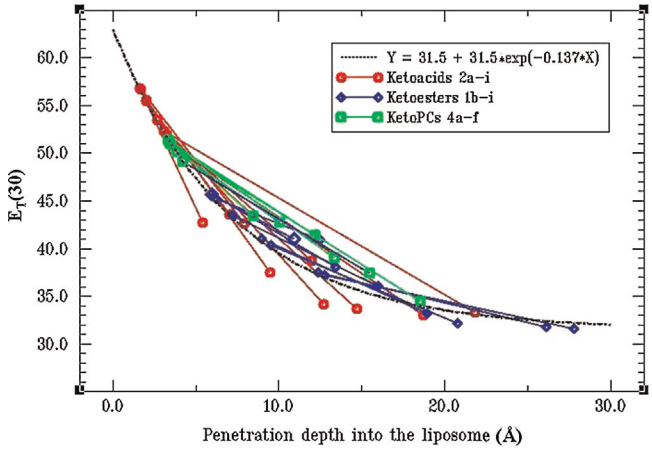

Fig. 8. ET(30) values experienced by the carbonyls in ketoester **1**, ketoacid **2** and ketoPCs **4** as a function of penetration depth (PD).

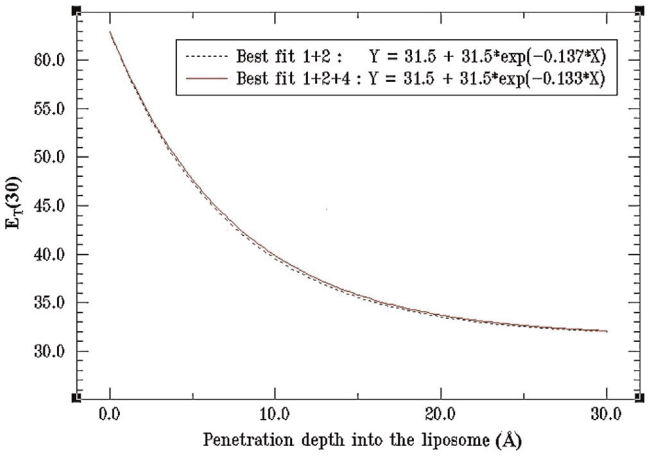

Fig. 9. Best fit curves for a plot of $E_T(30)$ values as a function of the penetration depth (PD) for: (··· ···) the carbonyls in ketoesters **1** and ketoacid **2;** and for (——) the carbonyls in ketoester, ketoacids and ketoPCs **1, 2** and **4**.

Table 6
Correlation between penetration depth within DMPC liposomes and the corresponding $E_T(30)$ polarity.

Å	$E_T(30)$	Å	$E_T(30)$	Å	$E_T(30)$
0	63.00	10	39.50	20	33.53
1	58.97	11	38.48	21	33.27
2	55.45	12	37.59	22	33.05
3	52.38	13	36.81	23	32.85
4	49.71	14	36.13	24	32.68
5	47.38	15	35.53	25	32.53
6	45.35	16	35.02	26	32.39
7	43.57	17	34.57	27	32.28
8	42.03	18	34.18	28	32.18
9	40.68	19	33.83	29	32.09

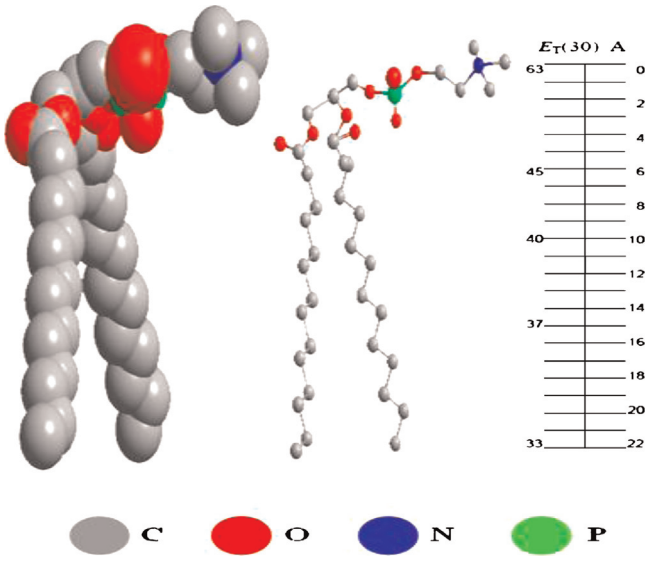

Fig. 10. Ruler for 1,2-dimyristoyl-*sn*-glycero-3-phosphatidylcholine (hydrogen atoms).

The above points, combined with Table 6, yields the chemical ruler shown in Fig. 10.

4. Conclusion

In the present paper, we have used bifunctional ketoesters **1**, ketoacids **2** and ketoPCs **4** to map various areas of the liposome. This in turn has made it possible to develop a molecular ruler by which the qualitative $E_T(30)$ polarity values can be converted to quantitative Å scale. The results show that the polarity in the liposome drops exponentially from a value of 63 kcal/mol near the lipid–water interface down to a value of ca. 33 kcal/mol at the midlayer of the DMPC bilayer at a depth of 22 Å. We turn now to demonstrate the applicability of this ruler to bioliposomes and biomembranes (e.g., erythrocyte ghosts).

Transparency document

The Transparency document associated with this article can be found in the online version.

Acknowledgements

We acknowledge the kind and generous support of the Israel Science Foundation (Grants Number 327/02 and 437/06) – founded by The Israel Academy of Sciences and Humanities, and The Ethel and David Resnick Chair in Active Oxygen Chemistry.

Appendix A. Supplementary data

Supplementary data associated with this article can be found, in the online version, at http://dx.doi.org/10.1016/j.chemphyslip.2014.07.003.

References

Afri, M., Alexenberg, C., Aped, P., Bodner, E., Cohen, S., Eigenberg, M., Eliyahu, S., Gilinsky-Sharon, P., Harel, Y., Naqqash, M.E., Porat, H., Ranz, A., Frimer, A.A., 2014. NMR-Based Molecular Ruler for Determining the Depth of Intercalants within the Lipid Bilayer. Part III: Studies on Keto-Esters and Acids. Chem. Phys. Lipids (companion paper).

Afri, M., Ehrenberg, B., Talmon, Y., Schmidt, J., Cohen, Y., Frimer, A.A., 2004a. Active oxygen chemistry within the liposomal bilayer Part III: Locating Vitamin E, ubiquinol and ubiquinone and their derivatives in the lipid bilayer. Chem. Phys. Lipids 131, 107–121.

Afri, M., Frimer, A.A., Cohen, Y., 2004b. Active 0xygen chemistry within the liposomal bilayer Part IV: Locating 2',7'-dichlorofluorescein (DCF), 2',7'- dichlorodihydrofluorescein (DCFH) and 2',7'-dichlorodihydrofluorescein diacetate (DCFH-DA) in the lipid bilayer. Chem. Phys. Lipids 131, 123–133.

Afri, M., Gottlieb, H.E., Frimer, A.A., 2002. Superoxide 0rganic chemistry within the liposomal bilayer. Part II:A correlation between location and chemistry. Free Radic. Biol Med. 32, 605–618.

Bodner, E., Afri, M., Frimer, A.A., 2010. Determining radical penetration into membranes using ESR splitting constants. Free Radic. Biol. Med. 49, 427–436.

Cohen, Y., Afri, M., Frimer, A.A., 2008a. NMR- based molecular ruler for determining the depth of intercalants within the lipid bilayer Part II: Quantitative values. Chem. Phys. Lipids 155, 114–119.

Cohen, Y., Afri, M., Frimer, A.A., 2008b. Aggregate formation in the intercalation of long chain fatty acid esters into liposomes. Chem. Phys. Lipids 155, 120–125.

Cohen, Y., Bodner, E., Richman, M., Frimer, A.A., 2008c. NMR?based molecular ruler for determining the depth 0f intercalants within the lipid bilayer. Part I: Discovering the guidelines Chem. Phys. Lipids 155, 98–113.

Frimer, A.A., Strul, G., Hameiri?Buch, J., Gottlieb, H.E., 1996. Can superoxide organic Chemistry be observed within the Liposomal Bilayer? Free Radic. Biol Med. 20, 843–852.

Matsudaira, P., Berk, A., Zipursky, S.L., Baltimore, D., Darnell, J., Lodish, H., 2000. Molecular Cell Biology, 4th ed W.H. Freedman, New York, pp. p159.

Menger, F.M., Richardson, S.N., Wood Jr., M.G., Sherrod, M.J., 1989. Chain-substituted lipids in monomolecular films. Effect of polar substituents on molecular packing. Langmuir 5, 833–838.

Ogg, R.A., Ray, J.D., 1957. Quadrupole relaxation and structures in nitrogen magnetic resonances of ammonia and ammonium salts J. Chem. Phys. 26, 1339–1340.

Reichardt, C., 1965. Empirical parameters of the polarity of solvents. Angew. Chem. Int. Ed. 4, 29–40.

Reichardt, C., 1994. Solvatochromic dyes as solvent polarity indicators. Chem. Rev. 94, 2319–2358.

Reichardt, C., Welton, T., 2011. Solvents and Solvent Effects Organic Chemistry, 4th ed. Wiley-VCH, Weinhein, Germany Chap. 6 and 7.

Shachan-Tov, S., Afri, M., Frimer, A.A., 2010. A reinvestigation of the reaction of coumarins with superoxide in the liposomal bilayer: correlation between depth and reactivity. Free Radic. Biol. Med. 49, 1516–1521.

Sassaroli, M., Vauhkonen, M., Perry, D., Eisinger, J., 1990. Lateral diffusivity of lipid analogue excimeric probes in dimyristoylphosphatidylcholine bilayers. Biophys. J. 57, 281–290.

Venable, R.M., Zhang, Y., Hardy, B.J., Pastor, R.W., 1993. Molecular dynamics simulations of a lipid bilayer and of hexadecane: an investigation of membrane fluidity. Science 262 (5131), 223–226.

Wiener, M.C., White, S.H., 1992. Structure of a fluid dioleoylphosphatidylcholine bilayer determined by joint refinement of X-ray and neutron diffraction data III. Complete structure. Biophys. J. 61, 434–447.